Photometric Signatures of Starbursts in interacting Galaxies and the Butcher-Oemler Effect

Karl D. Rakos

Inst. for Astronomy, Univ. of Vienna

Thomas I. Maindl

Inst. for Astronomy, Univ. of Vienna

and

James M. Schombert[1]

Infrared Processing and Analysis Center

Jet Propulsion Laboratory

California Institute of Technology

[1] Present Address: Astrophysics Division, NASA Headquarters, Washington, D.C. 20546

ABSTRACT

This paper present new and synthetic narrow band photometry of ellipticals, spirals, Seyferts and interacting galaxies in an attempt to identify the cause of the unusually high fraction of blue cluster galaxies in distant clusters (Butcher-Oemler effect). The properties and distribution of the low redshift sample specifically points to starbursts as the origin of the blue narrow band colors in interacting Arp galaxies. Comparison between theoretical models and multicolor diagrams, particular 4000Å break colors, indicates a photometric signature which differs from both normal disk galaxy star formation and nonthermal components. This photometric signature is absent for the Butcher-Oemler galaxies whose general color distribution, compared to present-day clusters, is consistent with a majority of the blue population involved in normal star formation rates (spiral- like) with the addition of a small fraction of bright, blue interacting/merger systems. This photometric picture of the Butcher-Oemler galaxies is in agreement with the morophological evidence from HST imaging.

Subject headings: galaxies: photometry - galaxies: starburst - galaxies: evolution

1. INTRODUCTION

Information gleaned from spectroenergy distribution (SEDs) of galaxies are kcy to our understanding of their age, metallicity, stellar population content and star formation histories. Analysis of SED data has usually invoked either population synthesis, which uscs a library of spectral templates (Pickles 1985), or evolutionary models, a method of convolving stellar isochrones with star formation rates and initial mass functions (Bruzual 1983, Arimoto and Yoshii 1986, Guiderdoni and Rocca-Volmerange 1987). In this series of papers (Fiala, Rakos and Stockton 1986; Rakes, Fiala and Schombert 1988; Rakos, Schombert and Kreidl 1991; Rakes and Schombert 1995), a system of narrow band filters have been used to replace the SED sampling at the sacrifice of resolution for a gain in signal-to-noise. And, just as stellar models arc tested by predictions of integrated quantities such as total luminosity, mass, radius and effective temperature, population synthesis results can then be tested by comparison to predictions of in tc.grated stellar content and metallicity of a galaxy as given by narrow Land indices. Thus, theoretical models, which produce spectra] energy distributions as a function of age, can be convolved to produce synthetic colors for comparison to narrow band observations at various redshifts.

Our project has approached this problem through the usc of a modified Strömgren filter system called uz, vz, bz, yz to distinguish it from the original *uvby* system. Our primary goal was to investigate the color evolution of ellipticals, testing the hypothesis that ellipticals arc the result of a single burst where all the stars formed at an epoch near the time of galaxy formation and later aged through passive stellar evolution. However, in the previous paper in this series (Rakos and Schombert 1995), the data revealed au extended Butcher-Oemler effect (the increasing fraction of blue to red galaxies in distant clusters) out to redshifts of 0,9 and containing up to 80% of the cluster population as blue galaxies (versus the previous values of 40% at red shift of *0.4)*. Deep HST images of intermediate redshift clusters (Dressler *et al.* 1994a,b) indicate that, while the brightest blue galaxies have disturbed morphologies suggestive of an origin of their blue colors from tidally induced star formation, a majority of the Butcher-Oemler galaxies have normal,]atc-type morpology. The goal of this paper is to combine the information obtained from narrow band photometry of nearby spirals, starburst, Seyferts and interacting galaxies in order to search for signatures of starburst activity that can then be linked to the uz, vz, bz, yz photometry of Butcher-Oemler galaxies in distant clusters.

The procedure used herein is fourfold. First, the uz, vz, bz, yz system will be linked to the original Strömgren system for stars to establish a baseline stellar sequence. Second, synthetic. colors for a range of galaxy types will be produced to map the behavior of the uz, vz, bz, yz system on galaxies with composite stellar populations and varying star formation histories. ‘1’bird, photometry of interacting/mergering galaxies will be presented to understand the signature of starburst phenomenon in galaxies. And lastly, comparison of the above data will be made to high redshift clusters to examine the hypothesis that blue cluster galaxies are the result of similar starburst activity.

2. PHOTOMETRIC PROPERTIES OF THE $uz,vz,,bz,yz$ COLOR SYSTEM

The Strömgren *uvby* filter system and its extensions (Strömgren 1966, *Wood* 1969) were developed to provide an accurate means of measuring the temperature, chemical composition and surface gravity of stars, without resorting to high resolution spectroscopy, by selecting regions of the stellar SED for narrow band photometry which are particularly sensitive to these specific properties. This provided an efficient and quantifiable method of sampling stellar types without the use of qualitative spectra] classification (e.g. the MK scheme).

The *uvby* system, modified for this project and designated as the uz, vz, bz, yz system, covers three regions in the near-UV and blue portion of the spectrum (see Figure 1 of Rakes and Schombert 1995). The first region is longward of 4600Å, where the influence of absorption lines is minor. This is characteristic of the bz (4650Å) and yz (5500Å) filters which produce a continuum color index, $bz - yz$, free of metal and surface gravity effects. The second region is a band shortward of 4600Å, but above the Balmer discontinuity. This region, covered by our vz (4 100Å) filter, is strongly influenced by metal absorption lines (i.e. Fe, CN) particularly for spectral classes F to M which dominate the contribution of light in galaxies. The third region is a band shortward of 4000Å, below the effective limit of crowding of the Balmer absorption lines, the so-called 4000Å break. The 4000Å break has been used by several studies as a measure of the evolution of galaxies (Hamilton 1985, Spinrad 1986, Dressler and Shectman

1987, Kimble *et al.* 1989) and the uz(3500Å) filter is a good measure of the blue side of this feature. The vz filter is in a good position to sample the red side of the 4000Å break with main transmission between 4050Å and 4250Å and, thus, the $uz - vz$ color is a convenient measure of this feature.

Our slight redefinition of the Strömgren system was primarily made to allow for a new definition of the blue side of the uz filter and to link the photometry system with the more reliable spectrophotometry standards that are now rapidly appearing in the literature. The original u passband in the Strömgren system is produced by the combination of the ultraviolet cutoff of the Earths atmosphere and a red blocking filter. But, as soon as the observations concern redshifted filters (such as distant clusters of galaxies, see Rakos and Schombert 1995), the transmission center of the filter is moved longward and, since the atmospheric cutoff does not redshift, the filter widens. Our solution is to substitute the original u filter by a 200Å wide interference filter, centered at the original u filter transmission) peak. However, the interference filter is slightly narrower than the original Strömgren u filter and produces a slight color term with respect to the new uz system (see below).

in this section, the uz, vz, bz, yz system will be related to the original Strömgren system for comparison to model atmospheres in the literature and to generate an understanding of the properties of the photometry system as it applies to the stellar populations in galaxies. There are two methods which can be used to derive the necessary transformations. First, the model atmospheres of Kurucz (1979) and Bell and Gustaffson (1978) can be convolved with the uz, vz, bz, yz filters and compared to the theoretical $uvby$ indices of those models in Lester *et al.* (1986). This first method was described in Rakos *et al.* (1991), but with only limited success due to the lack of range in stellar types.

The second method is to use spectrophotometric standards where the Strömgren indices are derived from spectrum scans. This second, and more realistic, method was performed by collecting 31 stars from the literature with known spectrophotometry and measured Strömgren photometry to form the transformations. The sample is from the IRS Standard Star Manual (Barnes and Hayes 1984) plus additional standards from Gunn and Stryker (1983). The Strömgren color indices are from Hauck and Mermilliod (1980). The resulting transformations are:

$$(bz - yz) = -0.268 + 0.937(b - y) \tag{1}$$

$$mz = -0.294 + 1.092m_1 - 0.017(b - y) \tag{2}$$

$$cz = 0.234 + 1.034c_1 - 0.152\,(b - y). \tag{3}$$

Note that m_1 and c_1 are the old Strömgren metal-line and surface gravity indices given as $m_1 = (v - b) - (b - y)$ and $c_1 = (u - v) - (v - b)$. The accuracy of the mz and cz transformations is ± 0.02 magnitudes.

As mentioned above, the amplitude of the 4000Å break is related to the $uz - vz$ color index. A comparison of the break values D_{4000} (Dressler and Shectman 1987) for the galaxies in §3 and the $uz - vz$ index reveals a linear regression of

$$2.5 \log D_{4000} = 0.646(uz - vz) + 0.245 \tag{4}$$

with a correlation coefficient of 0.91. The 4000Å break is correlated with effective temperature, surface gravity and metallicity in stars. However, for an integrated stellar population, it is primarily a temperature indicator (see Hamilton 1985 for a full discussion of the properties of the 4000Å break in stars and galaxies). Thus, the amplitude of the break is particularly sensitive to galaxy evolutionary effects such as the mean age of the stellar population (position of the main sequence turnoff point) and any recent epochs of massive star formation (presence of hot, young stars). This will also be the role of the $uz - vz$ index.

3. TWO-COLOR DIAGRAMS FOR THE uz, vz, bz, yz SYSTEM

The three primary stellar atmospheric parameters are surface gravity, metal content and temperature. These three parameters also dominate the integrated light from galaxies except that surface gravity becomes the ratio of dwarf to giant stars in the composite population and temperature becomes the mean age of the stellar population as given by the position of the turnoff point and the contribution of massive, young stars. Their combination determines our interpretation of multicolor photometry of galaxies as guided by models of galaxy evolution (see Tinsley 1980 for a review of the topic). The visual light from most normal galaxies is dominated by giants, with the low mass main sequence stars playing a minor role (Rose 1985). The metal content of most giant galaxies is between solar and 0.1 of solar (Schombert *et al.* 1993, Burstein 1985), in previous papers, it has been shown that the color index $bz - yz$ is relatively free of metal and surface gravity effects. The $vz - yz$ index is also free of surface gravity effects, but is sensitive to the metal content of a galaxy. In addition, the $uz - vz$, $uz - yz$ and mz indices can be used as a signature of hot stars (i.e. recent star formation and mean age) due to their sensitivity to the total near-UV flux of a galaxy,

In this section, the spectrophotometric data published by Gunn and Stryker (1983) has been used to build two-color diagrams for stars in our modified Strömgren system. Figures 1 and 2 display the synthetic colors for 162 standards of the Gunn-Stryker catalog. For $bz - yz$ vs $vz - yz$, an excellent correlation exists between these two colors, as would be expected, but this correlation is surprisingly independent of the mean surface gravity (i.e. stellar type). Note that the reddening vector is parallel to the star sequence. The derivation of the reddening vector according to Sinnerstad (1980) and Crawford (1975) is

$$E(c_1) = 0.20E(b - y) \tag{5}$$

and

$$E(m_1) = -0.32E(b - y) \tag{6}$$

from which it can be shown that

$$E(mz) = -0.39E(bz - yz) \tag{7}$$

$$E(cz) = 0.06E(bz - yz) \tag{8}$$

$$E(uz - vz) = 0.67E(bz - yz) \tag{9}$$

$$E(vz - yz) = 1.61\, E(bz - yz) \tag{10}$$

$$E(bz - yz) = 0.72E(B - V). \tag{11}$$

The ratio of total to selective absorption is 3.3, according to Moreno and Moreno (1 975), and it follows that

$$A(V) = 4.58E(bz - yz). \tag{12}$$

'J'bus, the reddening vector is parallel to the stellar sequence for $vz - yz$ vs $bz - yz$ and slightly orthogonal for $uz - vz$ vs $bz - yz$.

For these color indices, metallicity effects arc more dominant than surface gravity effects. Unfortunately, spcctrophotomctry of stars with low metal content is rare. To investigate the variance with metallicity, 35 stars were collected from the literature with the $[Fe/H]$ equal or less than --1.5 (Olsen 1983, Francois 1986, Magain 1987 and Tourkin *et al.* 1985) and their spectrophotometry was transformed to our color system. Within the range $0.2 < bz - yz < 0.8$ the color indices form a linear sequence such that

$$(vz - yz) = -0.227 + 2.524(bz - yz) \tag{13}$$

with a correlation coefficient of 0.97 (see solid line in the Figure 1). The difference in Figure 1 between the solar metallicity stars from the Gunn and Stryker spectrophotometric catalog is evident, but not overwhelming. Similar deviations for stars of different metal content in mz index is also present, but this was previous] y known from Strömgren photometry st u dies (see Gust affson and Del] 1978). Therefore, metallicity effects are not expect to strongly influence the discussions on star formation histories of galaxies.

The second set of two-color diagrams is the $uz - vz$ vs $bz - yz$ diagram also shown in Figure 1. Low temperature red giants arc well separated from dwarfs in Figure 1, but the stellar types become blurred for colors bluer than $bz - yz = 0.4$. The behavior of stellar types in this diagram is similar to broadband two color diagrams (e.g. Johnson UBV) with its classic "S" shaped sequence. The third and fourth set of two-color diagrams arc $bz - yz$ vs mz and $uz - vz$ vs mz, where the distributions arc identical for the various stellar types. However, note that the reddening vector is orthogonal to the stellar sequences in both diagrams.

For comparison to the stellar sequences, Figures 3 and 4 display the same diagrams for bright galaxies of various Hubble types. The galaxy data arc computed synthetic colors from high resolution, high signs]-to-noise spectra published by Gunn and Okc (1975), Yee and Okc (1 978), De Bruyn and Sargent (1 978), Kennicutt (1992a) and Ashby *et al.* (1 992). The galaxies arc broken into four classes; ellipticals, spirals, Seyferts and starbursts, and plotted as separate symbols in Figures 3 and 4. in general, for the $vz - yz$ vs $bz - yz$ plane, normal galaxies (ellipticals and spirals) follow the stellar sequence outlined in Figure 1. Seyfert galaxies arc bluer than spirals (the bluest objects arc all Seyferts), but lie near the stellar sequence. Note that the spectrophotometry from whit]] these synthetic colors arc based, have been observed with small aperture or slit sizes. Thus, these values arc strongly influenced by the nonthermal continuum component in Seyferts (the filters avoid most, of the strongest emission lines). Lastly, starburst galaxies deviate from the trend for normal and Seyfert galaxies by lying well below the stellar sequence, having bluer $vz - yz$ colors for their $bz - yz$ index (i.e. extra UV flux).

Dwarf stars arc numerous in galaxies and arc a dominate portion of the mass, but their integrated light has a minor influence on the total color of a typical bright galaxy (Rose 1985). The $uz - vz$ vs $bz - yz$ diagram is the most sensitive to changes, stellar types (main sequence to giants). However, the galaxy data displays little indication of any change in the dominate stellar type with respect to the integrated light. No differences between ellipticals and spirals arc distinguishable even though there arc extensive differences in their stellar populations.

For a reddening comparison, the position of a B0I star is marked in Figures 3 and 4 along with the reddening vector for that same star under 3 magnitudes of extinction. The data in Figures 3 and 4 confirms results from previous studies of starburst galaxies that their position in the $uz - vz$ vs $bz - yz$ dia.grain is similar to that of an object with a very young, hot stellar population shrouded in gas and dust. Under this interpretation, many of the starburst galaxies show a intrinsic reddening of between 0.5 to 3 mags of extinction.

in both mz plots for galaxies (see Figure 4), the starburst galaxies arc well separated from the normal ellipticals, spirals and Seyferts, and arc distinguished by consistently having mz values of less than –0.2. As with Figure 3, the reddening vector is shown with an origin of a B0Ia star and 3 magnit udcs of extinction. It is clear from these plots that the mz index provides the best signature for a starburst phenomenon in galaxies and both Figures 3 and *4* suggest that the narrow band optical properties of starburst galaxies arc dominated by a strongly reddened, young stellar population, as one would expect from their far-IR properties (see Devereux 1989).

The reddening of individual galaxies can be estimated using reddening free parameters introduced by Strömgren. The uz, vz, bz, yz photometric system has similar expressions:

$$[bz - yz] = (bz - yz) - 0.66E(B - V) \tag{14}$$

$$[uz - vz] = (uz - vz) - 0.67E(bz - yz) \tag{15}$$

$$[vz - yz] = (vz - yz) - 1.61E(bz - yz) \tag{16}$$

$$[mz] = mz + 0.39E(bz - yz) \tag{17}$$

$$[cz] = cz - 0.06E(bz - yz). \tag{Ifs}$$

]n this manner, an estimate of the unknown amount of reddening can be made and, therefore, our indices will only be dependent on the age and the total mass of the starburst. These arc still highly degenerate quantities, however, the color indices can be decoupled from the non-evolutionary properties of the galaxy.

4. uz, vz, 62, yz INDICES AND STARBURST MODELS

The dependence on age and burst strength of the underlying stellar population can be calibrated using theoretical models of starburst galaxies. 'l)o this end, the SED models of Leitherer and Heckman

(1 995) have been used to construct synthetic colors in order follow changes in the uz, vz, bz, yz color indices with the time.

To illustrate the changes in our four colors ($mz, uz - vz, vz - yz$ and $bz - yz$) two different models were considered. The first is a combination of a standard elliptical ($mz = -0.02$, $uz - vz = 0.89$; $bz - yz = 0.35$ and $vz - yz = 0.68$, see Schombert *et al.* 1993) with a starburst of total mass 106ikfo, solar metallicity, a Saltpeter IMF ($x = 2.35$) and an upper mass limit of 100 $M_{\odot}$. The evolution of the colors is shown in Figure 5 for three cases; one where the elliptical galaxy has the same total luminosity as the starburst (solid line), the second where the elliptical galaxy is one magnitude fainter than the starburst (dotted line) and the third where the elliptical galaxy is one magnitude brighter than the starburst (dashed line). Note that the luminosity, rather than burst mass, is used for normalization and the brightness of the burst is taken as the peak luminosity at 5500Å immediately after the start of the burst (t = 106 years). Several obvious trends are visible in Figure 5. All the color indices move progressively from blue to red as the burst ages, although this progression is not necessary smooth due to subtleties in the combination of the stellar tracks of various stellar masses. For example, there is a red bump at $\log t = 7.9$ due to a post-AGB phase. Another notable point is that both $vz - yz$ and $bz - yz$ approach the red color of an elliptical by 10^8 years of the initial burst, making starburst detection difficult in a relatively short time.

Surprisingly, the 4000Å break color, $uz - vz$, is the least sensitive index for detecting a past burst event. The $uz - vz$ color approaches an elliptical value after only approximatel y 107 years, independent of burst strength relative to the luminosity of the underlying population. Figure 1 in Rakes and Schombert (1 995), where the spectrum of an old composite population (17 Gyrs) is compared with one of a young population (1.5 Gyrs), depicts this effect. A strong, intermediate age population actually produces more flux in the vz band relative to the uz band due to a heavy Balmer contribution from A stars. This, in turn, implies a faster evolving $uz - vz$ index once the O and B stars become into red giants. This would also explain why the 4000Å break has produced mixed results as an indicator of galaxy evolution in low to intermediate redshift samples (see Dressler 1987) since an artificial reddening of the index would appear to mimic normal ellipticals if other colors were not measured for comparison. This is also evident in our previous work on high redshift cluster blue galaxies (Rakes and Schombert 1995). Figure 5 of that paper demonstrates that although the UV flux of this population changes dramatically beyond z = 0.6 (as measured by $uz - yz$), the $uz - vz$ colors are indistinguishable from the lower redshift galaxies. The red rise in $uz - vz$ colors at $\log t$ = 7.3 has a corresponding blue dip in $vz - yz$ and $bz - yz$ and indicates that blue galaxies are better selected by longer baseline continuum colors rather than 4000Å colors.

The mz index is the most sensitive of al] our indices to the existence of an underlying burst population having the largest magnitude change during the aging of the burst. And, significant differences are visible up to 5 x 108 years, providing a greater range of detection for the mz index. The sharp red bump at 10^8 years is due to a sudden onset of post giant branch supergiants from the initial burst, however, it's time phase is small. Notice this bump is stronger for a stronger burst due to a larger number of intermediate mass stars climbing the AGB.

The second experiment with the theoretical models of Leitherer and Heckman is the combination of a spiral, with constant star formation, and a burst as shown in Figure 6. In this example, the SB galaxy NGC 3227 was selected. NGC 3227 displays a moderate level of star formation (Kennicutt 1992b) with nominal colors of $mz = -0.05$, $uz - vz = 0.55$, $bz - yz = 0.22$ and $vz - yz = 0.39$. The three curves in Figure 6 are the same as in Figure 5 with the initial burst set to 1 mag below the luminosity of the spiral at 5500Å (dashed line), equal in luminosity (solid line) and 1 mag above (dotted line). The trends in Figure 6 are the same as was found for an elliptical plus star burst combination, however, the separation between the various burst strengths is less distinct in the early epochs due to the fact that the underlying population is already fairly blue from the constant disk star formation typical to a spiral. Again, note that the $uz - vz$ colors redden faster than any of the other filter combinations and that the stronger the burst, the redder the peak at $\log t = 7.3$, opposite to initial expectations for blue filters. Also, as with the elliptical plus starburst model, the 7712 index is the most sensitive to detecting a past starburst event. For both the elliptical and spiral underlying models, mz has the shallowest slope with time and will show evidence of a past starburst long after the other color indices have approached quiescent colors.

5. NARROW BAND PHOTOMETRY OF ARP/MARKARIAN GALAXIES

To confirm the previous sections results based on synthetic colors from spectrophotometry, new narrow band photometry, in the same filter sets as used for our high redshift work, was obtained for 13 Arp and Markarian galaxies. The sample, listed in Table 1, was selected based either on their far-IR, submillimeter or emission line properties to be systems of extremely high current rates of star formation and/or high molecular gas content, or by having a disturbed morphology suggestive of a recent merger of a gas-rich spiral (see Schombert *et al.* 1990). Table 1 presents the galaxies selected where column 1 displays the galaxy name, column 2 contains the galaxy coordinates (epoch 1950) and column 3 displays the galaxy redshift.

The CCD data for the Arp/Markarian sample were obtained on the Lowell observatory Hall (1.8m) and Perkins (1.1 m) telescopes. The imaging device on the 1.8m telescope was a TI 800 by 800 CCD with an image scale was 0.86 arcsecs per pixel. The 1.1 m telescope imaging device was a Tektronix 512 by 512 CCD also with an image scale of 0.86 arcsecs per pixel. The 1.8m observations were obtained on 1-4 Oct 1993. The 1.1 m observations were obtained 23-28 Jun 1994. All the Arp objects were imaged on the 1.8m telescope, the brighter Markarian galaxies were imaged on the 1.1 m telescope. Exposure times varied from 150 to 300 secs under photometric conditions with multiple frames per filter being co-added to increase the signal-to-noise and eliminate cosmic-ray events. Twilight flats were obtained for all four filters. The data were calibrated for both runs using the spectrophotometric standards HD 19445, HD 192281, Feige 15, BD+40 4032, BD+20 4211, HD 161817 and BD+26 2606 (Massey *et al.* 1988). Aperture photometry, centered on regions of peak intensity, was performed using the IRAF reduction package after erase line subtraction and flattening. Corrections for Galactic reddening followed the prescription of Burstein and Heiles (1978). Small k-corrections to final colors follow the procedure outlined in Fiala, Rakos and Stockton (1986). For the redshifts of the selected galaxies (see Table 1), these corrections were always less than 0.02 in mz. Isophotal maps from the yz images are presented in Figure 7.

In addition to the photometry of selected regions and the isophotal maps in Figure 7, yz surface brightness profiles of each galaxy where also analyzed. Due to the well-known irregular isophotal shapes of the sample galaxies, ellipse fitting was not prac.tics] or meaningful. Instead, a procedure of extracting wedge cuts along the minor and major axis was used. The purpose of these profiles is a simple comparison to an exponential or $r^{1/4}$ shape, not a full structural analysis. As an illustration, the profile for Arp 169 B and C, two $r^{1/4}$ profiles, is plotted in Figure 8.

The photometry can be found in ‘J’able 2 where the galaxy region designation from Figure 7 is listed in column 1, aperture size in pixels in column 2, uz - vz color in column 3, vz — yz color in column 4, $bz - yz$ color in column 5 and mz in column 6. Aperture photometry is used in this study since the synthetic colors from spectrophotometry is predominately from small slits or apertures centered on the highest surface brightness regions. We also used primitive circular aperture photometry for our high redshift clusters duc to the lack of spatial information, so comparison to those samples necessitates a similar reduction method. Typical errors where 0.05 in uz — vz, 0,02 in bz -- yz, 0,03 in vz -- yz and 0.04 in mz. The following arc remarks to’ photometry of the individual galaxies in the sample:

Arp 81: Figure 7 shows the two interacting galaxies that make up this system. The galaxy labeled E has the photometric signature of regular E galaxy in terms of mean colors and a surface brightness profile that is pure $r^{1/4}$. ‘l’he second galaxy B has the appearance of a bared spiral disturbed by a neighbor. At the center, the galaxy has a nuclear hotspot that the uz filter indicates an unusual number of hot stars. ‘l’he region A is also active (blue in mean color) but not within the definition of a strong starburst phenomenon, but rather a buried AGN is indicated (scc Bushouse 1987).

Arp 112: Both galaxies A and B display signatures of a star forming system and strong intrinsic absorption based on their positions in the two color diagrams. The galaxy A has exponential surface brightness profile. Galaxy B has an irregular profile shape.

Arp 118: Both galaxies A and B have general $r^{1/4}$ profile shapes with some irregularity present. Colors arc characteristic of a starburst in its late stages (greater than 0^{8} years). The central region is known to harbor a Seyfert type 2 nuclei (Hippelein 1989).

Arp 157: Galaxy A appears unobscured, however, galaxy C is hidden behind a dust lane, consistent with their colors. Both are involved in an intense starburst event. The galaxy A has a partly disturbed $r^{1/4}$ profile. The whole system is a luminous IRAS source (Young *et al. 1989).*

Arp 169: Both galaxies B and C are typical ellipticals without any signature of recent star formation in their mean colors (see also Schombert *et al.* 1990). The brightness profiles for both systems are pure $r^{1/4}$ (see Figure 8).

Arp 182: The photometry in the *uz* band was disturbed by weather. However, galaxies A and B show the presence of hot stars and dust in the centers based on the redder filters. The galaxy A has a disturbed brightness profile, B has a $r^{1/4}$ profile outside the inner 5 arcsecs.

Arp 212: Arp 212 is a well-studied starburst galaxy (Devereux 1989) with exponential profile (disk-like). The narrow band colors indicate a strong starburst with equally strong dust extinction in the bulge as confirmed by far-IR emission.

Arp 223: Although Arp 223 has a disturbed morphology (a classic shell/merger galaxy, see Schombert *et al. 1990),* its narrow band colors are similar to a normal elliptical. Given the structural signatures of a recent merger, Arp 223 is a probable late stage starburst with a mean age greater than 108 years.

A **rp** *278:* Unfortunately, the *uz* observations for this galaxy were lost to weather. However, the starburst signature is present in many of the bright knots embedded in both galaxies based on vz, bz and yz colors. Knot G has, in comparison to other regions in the interacting system, the highest reddening due to dust.

A **rp** 282: This galaxy pair have dramatically different colors. Galaxy A has very blue, star-forming colors. Galaxy B displays the colors of a reddened elliptical, yet has a disk morphology.

Mrk 309: This galaxy is known in the literature as a typical WR galaxy (Conti 1991) and displays the bluest colors of our sample. It is a blue compact galaxy with a $r^{1/4}$ profile. A majority of the surface area of the galaxy is involved in massive star formation.

Mrk 480: This system is most probably a merging galaxy pair, both disk galaxies based on their exponential profiles. Both galaxies show fading starburst signatures of intermediate mass B and A stars (Mazzarella and Boroson 1993).

Mrk 496: This galaxy has two compact, blue nuclei with only moderate intrinsic absorption based on very blue $uz - vz$ colors. The surface brightness profile is exponential in the interior and irregular at the edge. This galaxy is an ultraluminous IRAS source (log $L_{FIR}/L_{\odot} = 11.33$, Condon *et al.* 1991).

Figures 9 and 10 display the photometry for the Arp/Mrk sample in the same fashion as Figures 1 through 4. The photometry for different apertures of the same objects are connected by lines. Also shown on the diagrams are boxes that outline the 90% regions for ellipticals, Seyferts and starburst galaxies from Figures 3 and 4. There is a small trend of blue gradients in $vz - yz$, $bz - yz$ and mz. The exception to this trend is found in the $uz - vz$ vs $bz - yz$ diagram where redder $uz - vz$ indices are found for bluer $bz - yz$ (see discussion in §4).

The main result from Figures 9 and 10 is that a majority of the Arp/Mrk objects occupy the same region of the two color diagrams that the starburst sample defined. This confirms our interpretation of the narrow band colors, particularly the mz differences for starburst galaxies, in their ability to detect a photometric signature of a starburst versus AGN activity or normal disk star formation (constant SFR). A significant fraction (25%) have elliptical-like colors and profile shapes (i.e. $r^{1/4}$), however, it should be noted that several of the Arp objects appear to be interactions between ellipticals and spiral disks. In Figure 10, the elliptical plus starburst tracks from Figure 5 are plotted in the mz plane (dotted line corresponding to the equal luminosity model). Many of the starburst colors are consistent with ages of 107 years or younger, if notable reddening is present, which is in agreement with dynamical models of the star formation history of interacting galaxies (Mihos and Hernquist 1994). The mz vs $uz - vz$ diagram indicates that many of the red objects could be old starbursts with ages of greater than 10^8 years, Outside of blue elliptical colors and weak starburst indices, only one galaxy (Arp 81A) displays consistent Seyfert colors (Arp 118, a known Seyfert 2, lies on the boundary between ellipticals and Seyferts). The lack of Seyfert colors is probably due to contamination and mixture of stellar populations that occurs with the wider aperture sizes compared to the narrower slits of' the spectroscopy surveys.

6. STARBURSTS AND THE BUTCHER-OEMLER EFFECT

From the theoretical models in §4 plus the synthetic colors from spectrophotometry and new photometry of Arp/M rk galaxies presented in §5, a fair] y consisten t pictu re is outlined for the photometric signature of a starburst event, old or new, in a composite stellar population. Although blue $vz - yz$ and $bz - yz$ colors arc found in starburst galaxies, reddening distorts the interpretation of the colors with respect to age and strength of the burst. The $uz - vz$ or 4000Å index is a good measure for very you ng st arbu rsts, however, intermediate mass stars produce artificial] y red colors (scc §4). The most powerful indicator, as seen in Figure 4, is the mz index where a value less than – 0.2 indicates a starburst regardless of reddening. The mz index is also the most sensitive to detecting old starbursts hidden within an elliptical population since it more sensitive to turnoff stars and evolves slowly from the time of the initial burst (see Figure 5).

Figure 11 displays the mz values for the ellipticals, spirals, Seyfert and starburst spectrophotometry of §3 (mean values arc indicated by an arrow at the top of each histogram). Although there is some overlap in the range of mz values for each galaxy type, the ellipticals have the reddest mz value of 0.02 and starbursts fall at the blue end of –0.29. Spirals and Seyferts have mean values between –0.05 and –0.1 O. Also shown in Figure 11 arc the data from Rakes and Schombert (1 995) for the distant cluster sample divided into two redshift bins at the top right, and the $z > 0.6$ galaxies divided by $bz - yz$ color into red and blue galaxies (scc that paper for a full description of the sample). The Butcher-Oemler galaxies ($z > 0.6$ blue galaxies in the bottom right panel of Figure 11) have a mean color indistinguishable from the mean for the spiral sample. However, the distribution of Butcher-Oemler galaxies differs from the normal spirals distribution by having a notable blue tail. Wc also note that the bluest Butcher-Oemler galaxies are often the brightest galaxies in their respective clusters.

The extreme blue members of this color distribution must attribute their colors to a starburst phenomenon since neither spirals or Seyferts in the low redshift sample display these colors. 'J'his is an important distinction since spectroscopy surveys of distant clusters have isolated a high fraction of cluster galaxies with strong emission lines (Dressler and Gunn 1983) which offers an alternative explanation of the Butcher-Oemler effect in terms of either high levels of current star formation (i.e. strong emission from HII regions) or increased AGN phenomenon with higher redshift. Our uz, vz, bz, yz filter system specifically avoids the dominant emission lines in AGN activity and focuses on the underlying continuum emission from the hot gas and stellar populations. Thus, the lack of agreement in mz with the Seyfert samples would discount the AGN effects in favor of strong star formation as the explanation for the Butcher-Oemler effect.

This photometric result is consistent with the recent morphological results from HST imaging of $z = 0.4$ clusters by Dressler *et al.* (1994 a, b). In that study it was found that, while some of the brightest blue galaxies showed evidence of enhanced star formation due to tidally effects or mergers, most of the blue cluster galaxies are normal, late-type spirals and irregulars, Their blue colors being due to normal star formation rates and histories. The number of disturbed systems, ones which had clearly undergone a recent tidal encounter or full merger, is higher in these distant clusters as compared to present-day cluster populations, but represent less than 10% of the cluster population. Dressler *et al.* *(1994b)* also notes that the morphologically disturbed systems are the brightest blue galaxies, supporting a starburst interpretation for their origin.

The morphological information combined with our photometric results indicated that the color distribution of the Butcher-Oemler galaxies in Figure 1 j are due to two components. The first. is a sequence of morphological y late-t ype galaxies with normal star formation rates and histories. The second component is a blue tail composed of galaxies with starburst colors and disturbed morphologies. We also note that the $uz - vz$ or 4000Å break colors of the high redshift blue cluster gal ax ics are not as strongly blue as compared to the continuum colors (e.g. $uz - yz$ or $bz - yz$). The theoretical models of Leitherer and Heckman (1 995) demonstrate that this is the result of a increasing contribution from intermediate mass stars (A and F t ype) as t] ıe starburst ages. This produces artificially reel 4000Å break colors when, in reality, the UV flux is still quite high from young stars. This would *also explain* Hamilton (1985) observation that there is little evolution in the 4000Å break colors of high redshift, color- selected field galaxies in terms of a lack of h igh mass O and B stars rather than a lack of color evolution.

7. CONCLUSIONS

Rakos and Schombert (1995) demonstrated that Butcher-Oemler effect is much more dramatic than previous thought. Early work on cluster galaxies found blue fractions from 30 to 40% in clusters with redshifts of 0.4. Rakes and Schombert found fractions of 80% in clusters at redshifts of 0.9. This is a very dominate effect on cluster populations not only in terms of the rapid pace of galaxy evolution as first observed by Butcher and Oemler, but also in the extent of the blue galaxy population prevails over the entire cluster population at high redshifts (80% would imply all present-clay SO's are actively star-forming at these epochs).

In this paper we have derived and described the fundamental properties of the uz, vz, bz, yz filter system. In particular, wc have demonstrated the advantage of mz index as a detector of starbursts in galaxies. Wc then applied this index to establish the photometric signature of starbursts in interacting galaxies. This method was then applied to high redshift clusters to demonstrate that the Butcher-Oemler galaxies are due to a mixture of star-forming spirals and irregulars plus an addition component from a small fraction of starburst galaxies.

The following is a summary of our primary results and interpretations:

(1) The uz, vz, bz, yz filter system is a robust tool for exploring the stellar populations in galaxies due to the placement of the filter centers in regions of clearer evolutionary interpretation. The narrow width of the filters avoids contaminating emission lines so as to concentrate on the underlying continuum emission from stellar atmospheres or nonthermal emission.

(2) The uz, vz, bz, yz system is relinked to spectroscopy standards and the transformations from the original Strömgren system are derived. The reddening effects are outlined and displayed in Figures 1 and 2.

(3) Using spectrophotometry of ellipticals, spirals, Seyferts and starburst galaxies from the literature, synthetic uz, vz, bz, yz indices are produced and plotted on multi-color diagrams. Specific regions are

occupied by various, galaxies types and the mz index is demonstrated as the best indicator of starburst activity.

(4) Theoretical models from Leitherer and Heckman are used to define the behavior of the uz, vz, bz, yz indices with time from the initial starburst. The inadequacy of the 4000Å break color, $uz - vz$, is shown due to the contribution of intermediate mass stars to an aging burst. Again, the mz index is shown to be the most sensitive to starburst activity and for the longest amount of time post-starburst.

(5) New photometry for a sample of Arp and Markarian galaxies is presented and confirms the results from the synthetic colors that starburst galaxies have a unique, detectable signature in the uz, vz, bz, yz system. Selection by disturbed morphology also confirms the dynamical arguments for starbursts in merger/interacting galaxies.

(6) Direct comparison with the photometry of blue galaxies in distant clusters (z > 0.6) yields the interpretation that the Butcher-Oemler effect is due primarily to normal star formation with a small component due to tidally induced starbursts. The recent results from HST imaging (Dressler *et al.* 1994a,b) confirms this interpretation and suggests that the Butcher-Oemler effect is a indicator of dynamical evolution as well as color evolution.

The authors wish to thank the director and staff of the Lowell Observatory for granted time for this project. Financial support from the Austrian Fonds zur Foerderung der Wissenschaftlichen Forschung is gratefully acknowledged. We also wish to thank C. Leitherer for synthetic spectra of starburst galaxies and R. Kennicut, A. De Bruyn and M. Ashby for numerical values of measured spectra of galaxies. This research has made use of the NASA/IPAC Extragalactic Database (NED) which is operated by the Jet Propulsion Laboratory, California Institute of Technology, under contract with the National Aeronautics and Space Administration.

References

Arimoto, N. and Yoshii, Y. 1986, *Astron. Astrophys.*, 164, 260.

Ashby, M., Houck, J. and Hacking, P. 1992, *A. J., 104, 980.*

Barnes, J. and Haynes, I). 1984, *IRS Standard Star Manual* (Tucson: Kitt Peak National Observatory).

Bell, R.A. and Gustaffson, B. 1978, *Astron. and A strophys. Suppl., 34, 229.*

Bruzual, A.G. 1983, *Ap.J., 273, 105,*

Burstein, D. and Heiles, C. 1978, *Ap.J.*, 225, 40.

Burstein, 1). 1985, *P.A.S.P.*, 97, 89.

]] US]1OUSC, 11.1987, *Ap.J.*, 320, 49.

Condon, J., Huang, Z., Yin, Q. and Thuan, 'i'. 1991, *Ap.J., 378, 65.*

Conti, 1'.1991, *Ap.J., 377, 115.*

Crawford, D.L. 1975, *P. A. S.P.*, 8'7, 481.

Dc Bruyn, A. and Sargent, W. 1978, *A. J.*, 83, 1257.

Devereux, N. 1989, *Ap.J., 346, 126.*

Dressler, A. and Gunn, J. 1983, *Ap.J., 270, 7.*

Dressler, A. 1987, in Nearly Normal Galaxies from the Plank Time to the l'resent, cd. S. Faber (New York: Springer-Vcrlag), p. 265.

Dressler, A. and Shectman, S. 1987, *A .J.*, 94, 899.

Dressler, A., Oemler, A., Butcher, H. and Gunn, J. 1994a, *Ap.J., 430, 107.*

Dressler, A., Oemler, A., Sparks, W. and Lucas, R. 1994b, *Ap.J., 435, 23.*

Fiala, N., Rakos, K.D. and Stockton, A. 1986, *P.A.S.P.*, **98**, 70.

Francois, P., 1986, *Astron. Astrophys.*, **160**, 264.

Guiderdoni, B. and Rocca-Volmerange, B. 1987, *Astron. Astrophys.*, 186, 1.

Gunn, J.E. and Oke, J.B. 1975, *Ap.J.*, 195, 255.

Gunn, J.E. and Stryker, L.L., 1983, *Ap.J. Suppl.*, *52, 121.*

Gustaffson, B. and Bell, R.A. 1979, *Astron. Astrophys.*, 74, 313.

Hamilton, D. 1985, *Ap.J.*, *279, 371.*

Hauck, B. and Mermilliod, M., 1980, *Ap.J. Suppl.*, *40,* 1.

Hippelein, H. 1989, *Astro. Astrophys.*, 216, 11.

Kennicutt, R. 1992a, *Ap.J. Suppl.*, *79, 255.*

Kennicutt, R. 1992b, *Ap.J.*, *388, 310.*

Kimble, R. A., Davidsen, A.F. and Sandage, A.R. 1989, *Astrophys. and Sp. Se.*, *157,* 237

Kurucz, R.L. 1979, *Ap.J. Suppl.*, *40,* 1.

Leitherer, C. and Heckman, T.M. 1995, *Ap. J. Suppl.*, *96,* 9.

Lester, J.B., Gray, R.O. and Kurucz, R.L. 1986, *Ap.J. Suppl.*, 61, 509.

Massey, P., Strobel, K., Barnes, J. and Anderson, E. 1988, *Ap. J.*, *328, 315.*

Magain, P., 1987, *Astron. Astrophys.*, *179,* 176.

Mazzarella, J. and Boroson, T, 1993, *Ap.J. Suppl.*, *85, 27.*

Mihos, C. and Hernquist, L. 1994, *Ap.J. Letters*, *431, 1,9.*

Moreno, A.G. and Moreno, H. 1975, *P.A.S.P.*, 87, 425.

Olsen, H., 1983, *Astron. Astrophys. Suppl.*, *54, 55.*

Pickles, A.J. 1985, *Ap.J. Suppl.*, *59, 33.*

Rakos, K.D., Fiala, N. and Schombert, J.M. 1988, *Ap.J.*, *328, 463.*

Rakos, K.D., Schombert, J.M. and Kreidl, T.J. 1991, *Ap.J.*, *377, 382.*

Rakos, K.D. and Schombert, J.M. 1995, *Ap.J.*, *439, 47.*

Rose, J. 1985, *A.J.*, 90, 1927.

Schombert, J., Wallin, J. and Struck-Marcell, C. 1990, *A. J., 99, 497*

Schombert, J., Hanlan, P., Barsony, M. and Rakes, K. 1993, *A .J.*, 106, 923.

Sinnerstad, U. 1980, *Astro. Astrophys. Suppl.*, 40, 395.

Spinrad, H. 1986, *P.A.S.P.*, 98, 269.

Strömgren, B. 1966, *Ann. Rev. Astron. Astrophys., 4, 443.*

Tinsley, B. 1980, *Fundam. Cosmic Phys., 5, 287.*

Toukin, J., Lambert, D.L. and Balachandran, S. 1985, *Ap.J.*, 290, 289.

Wood, D.B. 1969, *A. J., 74, 177.*

Yee, H.K.C. and Oke, J.B. 1978, *Ap.J., 226, 753.*

Young, J., Xie, S., Kenney, J. and Rice, W. 1989, *Ap. J. Suppl., 70, 699.*

Table 1. Arp/Markarian Galaxies

Name	R.A. (1950)	Dec.	V_{hel}
ARP 81 NGC 6621,22	1813.4	+68 18	6243
ARP 112 NGC 7805,6	2359.9	+31 17	5125
ARP 118 NGC 1143,44	0253.6	–00 17	8531
ARP 157 NGC 520	0123.0	+03 38	2281
ARP 169 NGC 7236	2213.3	+13 42	7886
ARP 182 NGC 7674	2326.3	+08 37	8698
ARP 212 NGC 7625	2319.0	+17 04	1633
ARP 223 NGC 7585	2316.4	–04 49	3447
ARP 278 NGC 7253	2218.1	+29 14	4873
ARP 282 NGC 169	0035.3	+23 50	4593
MRK 309	2250.2	+24 28	12636
MRK 480	1504.7	+42 50	5765
MRK 496 NGC 6090	1610.4	+52 35	8785

Table 2. Photometry of Arp/Markarian Galaxies

Name		D	uz − vz	bz − yz	vz -- yz	mz
ARP 81	A	5	0.32	0.24	0.36	--0.12
	A	10	0.35	0.17	0.33	–0.01
	B	5	0.41	0.39	0.60	–0.18
	B	10	0.37	0.34	0.52	--0.16
	E	5	0.90	0.42	0.84	+0.00
	E	10	0.93	0.39	0.77	–0.01
ARP	112A	5	--	0.52	0.91	–0.18
	A	10	--	0.43	0.81	--0.05
	A	20	--	0.41	0.75	–0.07
	B	5	0.53	0.59	1.00	–0.18
	B	10	0.69	0.49	0.89	-0.09
	B	20	0.74	0.45	0.87	–0.03
ARP	118A	5	0.65	0.37	0.85	+ 0.11
	A	10	0.73	0.34	0.73	+0.05
	B	5	0.74	0.49	0.92	–0.06
	B	10	0.7'2	0.42	0.76	--0.08
ARP	157A	10	0.42	0.20	0.19	–0.21
	A	15	0.48	0.31	0.30	-0,32
	A	20	0.53	0.31	0.29	–0.33
	C	5	---	0.25	0.25	-0.25
	c	10	--	0.39	0.47	–0.31
ARP	169B	5	0.60	0.44	0.95	-1-0.07
	B	10	0.90	0.37	0.85	+0.11
	C	5	0.62	0.46	0.98	+0.06
	C	10	0.60	0.37	0.86	+0.12
ARP1	82A	3	--	0.29	0.31	--0.27
	A	5	--	0.26	0.32	–0.20
	A	10	--	0.25	0.36	–0.14
	B	3	--	0.41	0.52	–0.30
	B	5	--	0.37	0.51	–0.23
	B	10	--	0.32	0,50	--0.14
ARP	212	3	--	0.35	0.45	–0.25
		5	0.35	0.31	0.40	–0.22
		10	0.37	0.26	0.36	--0.16
		25	0.31	0.24	0.34	--0.14
ARP	223	5	0.90	0.31	0.63	+0.01
		IO	0.85	0.30	0.58	–0.01
		15	0.82	0.30	0.57	--0.03
		25	0.78	0.29	0.55	–0.03

Table 2. (continued)

Name	D	$u_z - v_z$	$b_z - y_z$	$v_z - y_z$	m_z
ARP 278B	5	–	0.36	0.44	–0.28
B	10	–	0.34	0.46	–0.22
C	5	–	0.47	0.61	–0.33
D	5	–	0.23	0.30	–0.16
F	5	–	0.27	0.26	–0.28
G	5	–	0.78	1.26	–0.30
H	5	–	0.37	0.51	–0.23
ARP 282A	3	0.25	0.15	0.17	–0.13
A	5	0.35	0.13	0.15	–0.11
A	10	0.42	0.12	0.19	–0.05
B	3	0.86	0.58	1.11	–0.05
B	5	0.93	0.59	1.11	–0.05
B	10	1.06	0.58	1.06	–0.10
MRK 309	5	–0.17	0.10	–0.05	–0.25
	10	–0.04	0.13	–0.04	–0.29
	15	0.03	0.14	0.02	–0.26
	20	0,00	0.13	0.07	–0.19
MRK 480A	10	0.62	0.14	0.06	–0.22
A	15	0.53	0.15	0.13	–0.17
B	10	0.44	0.16	0.11	–0.21
B	15	0.49	0.16	0.13	–0.19
MRK 496	10	0.13	0.13	0.05	–0.21
	15	0.20	0.11	0.04	–0.18
	20	0.24	0.12	0.06	–0.18

Figure Captions

Figure 1. Two color diagrams for the Gunn-Stryker standard stars. Circles arc main sequence stars, solid symbols arc stars of luminosity class IV and stars arc stars of luminosity class 111. The solid line represents the position of metal poor stars, see text. The reddening vector for onc magnitude of extinction is shown.

Figure 2. The mz index diagrams for the Gunn-Stryker standard stars. Symbols arc the same as Figure 1,

Figure 3. Two color diagrams for the synthetic colors of galaxies with spectrophotometry from the literature. The four classes of galaxies; ellipticals, spirals, Seyferts and starbursts, arc shown with the reddest objects being ellipticals and the bluest being Seyferts in continuum emission. The position of a B01 star and 3 magnitudes of reddening arc also shown. Note that starburst galaxies following the reddening curves from a young or intermediate age stellar population.

Figure 4. The mz index diagrams for the synthetic. colors of galaxies with spectrophotometry from the literature. Starburst galaxies occupy a specific region in the mz plane with values at least lcss than --0.2.

Figure 5. The starburst models of Leitherer and Heckman combined with a typical elliptical population. Three combinations arc shown; equal luminosity between elliptical and starburst maximum (solid line), onc magnitude fainter for the starburst (dotted line), onc magnitude brighter (dashed line). The mz index is the most sensitive to old starburst detection. The 4000Å break color, $uz - vz$ is the least sensitive to an aging starburst.

Figure 6. The starburst models of Leitherer and Heckman combined with a typical spiral population. Lines arc the same as in Figure 5. The colors of the starburst approach normal spiral colors in only 5×10^7 yrs.

Figure 7. Isophotal maps of the Arp/Markarian sample. All images arc yz band with aperture photometry regions from 'Table 2 marked.

Figure 8. Surface brightness profiles for Arp 169 A and B. Note the $r^{1/4}$ shape (straight line) typical for an elliptical galaxy.

Figure 9. Two color diagrams for the Arp/Markarian sample. Regions from Figure 3 are marked for three galaxy classes: ellipticals, Seyferts and starbursts. Different sized apertures are connected by lines.

Figure 10. The mz diagrams for the Arp/Markarian sample. The dotted line is the equal luminosity starburst model from Figure 5. Note that a majority of the Arp/Markarian sample lies in the starburst region of the diagram.

Figure 11. Histograms for the mz values of ellipticals, sprials, Seyferts and starburst galaxies are compared to the data from intermediate and high redshift cluster galaxies, The Butcher-Oemler galaxies (z >0.6 blue galaxies) display a similar color distribution to the present-day sprial sample with an additional blue tail due to a small fraction of starburst galaxies.

Thomas I. Maindl: Astronomisches Institut, University Observatory, Turkenschanzstrasse 17, A- 1180, Wien, Austria

Karl D. Rakes: Astronomisches Institut, University observatory, Turkenschanzstrasse 17, A-1 180, Wien, Austria

James M. Schombert: Astrophysics Division, NASA Headquarters, 300 E St., S. W., Washington, D.C. 20546

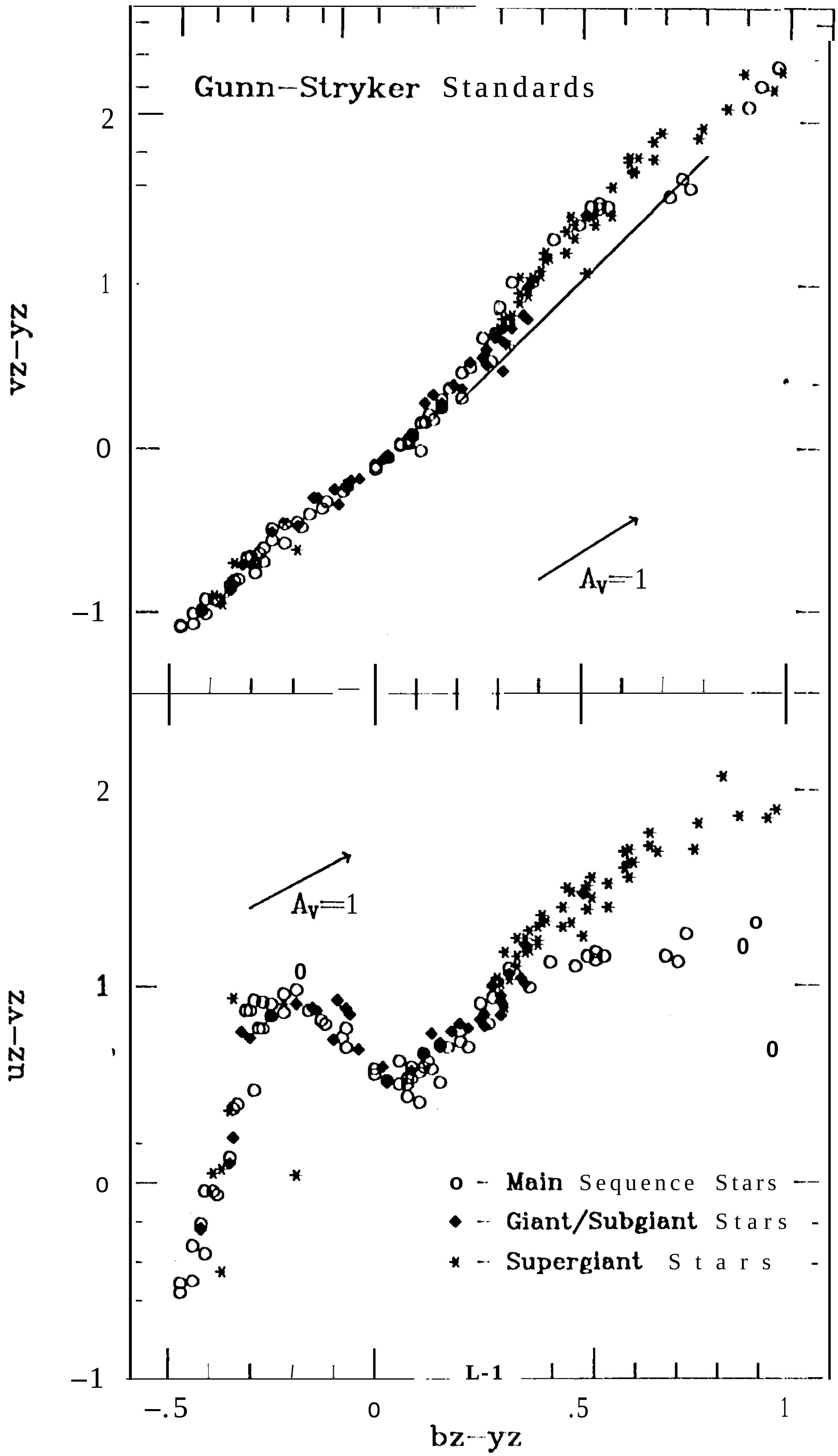
Gunn–Stryker Standards
vz–yz
uz–vz
bz–yz
$A_V=1$
$A_V=1$
o – Main Sequence Stars
◆ – Giant/Subgiant Stars
* – Supergiant Stars
2
1
0
−1
2
1
0
−1
−.5
0
.5
1

Figure 1

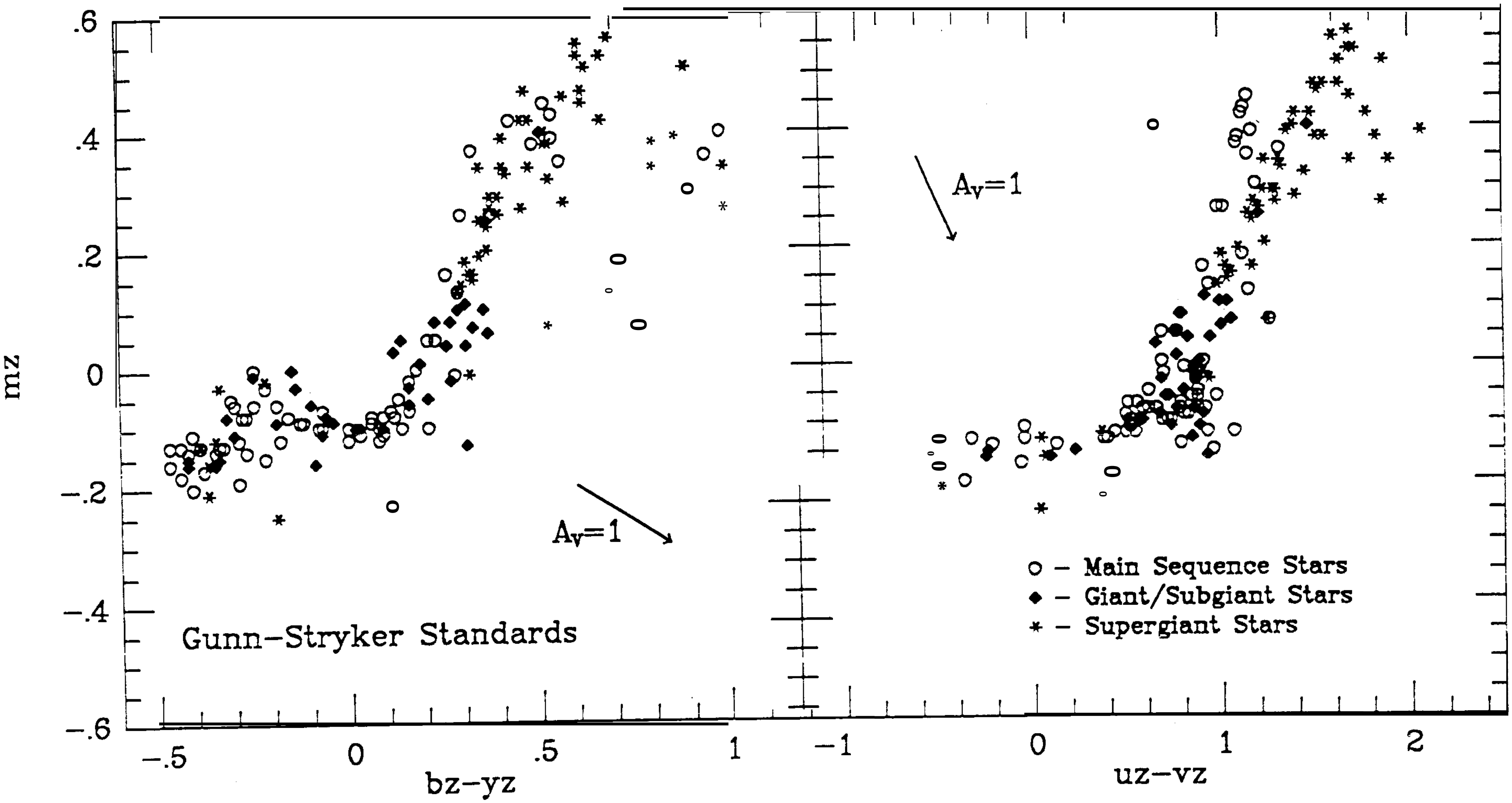
mz
.6
.4
.2
0
-.2
-.4
-.6
-.5
0
.5
1
bz-yz
-1
0
1
2
uz-vz
$A_V=1$
$A_V=1$
Gunn-Stryker Standards
o – Main Sequence Stars
◆ – Giant/Subgiant Stars
* – Supergiant Stars

Figure 2

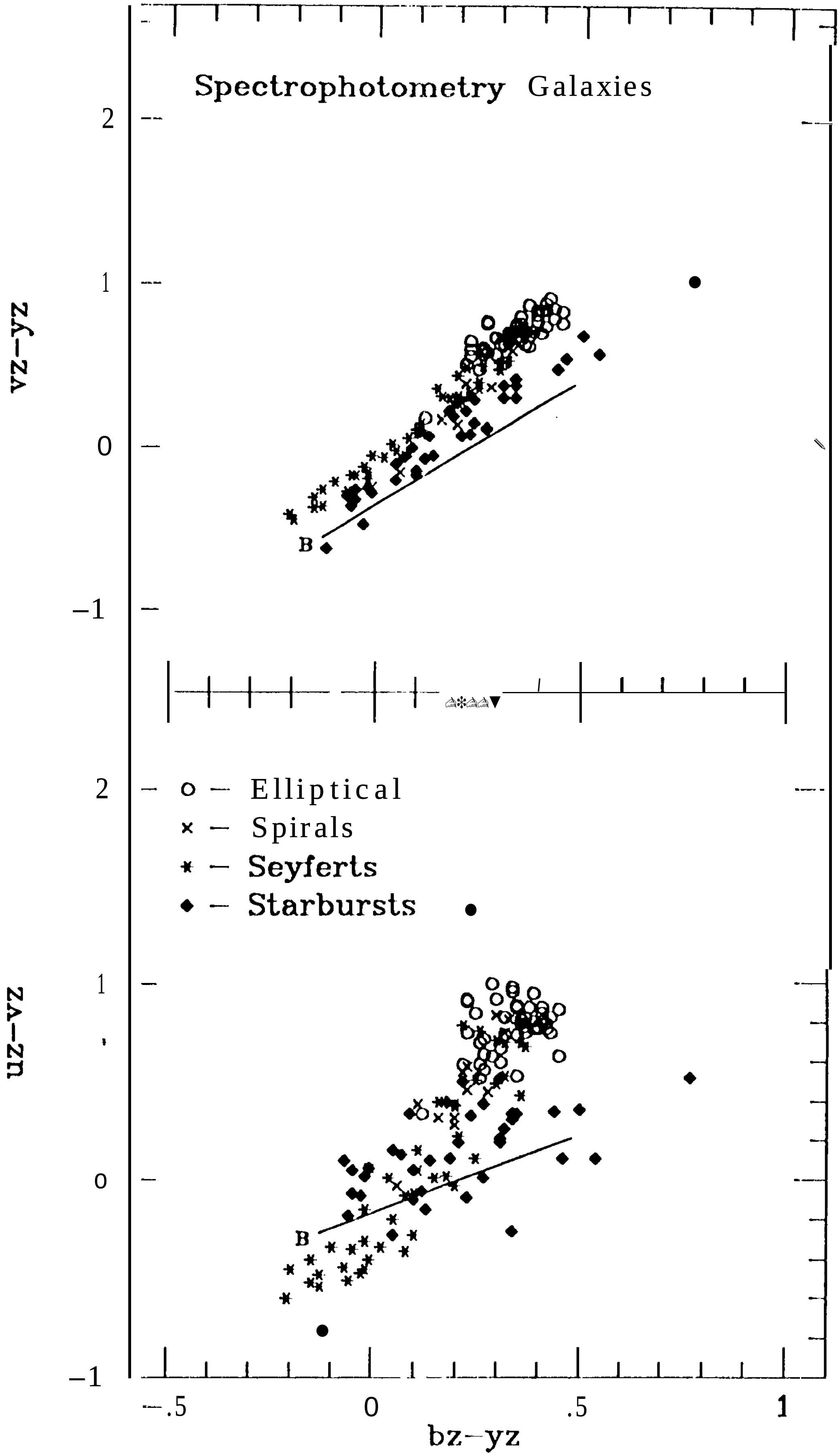
Spectrophotometry Galaxies
vz−yz
uz−vz
bz−yz
o − Elliptical
× − Spirals
∗ − Seyferts
◆ − Starbursts
B
2
1
0
−1
−.5
.5

Figure *3*

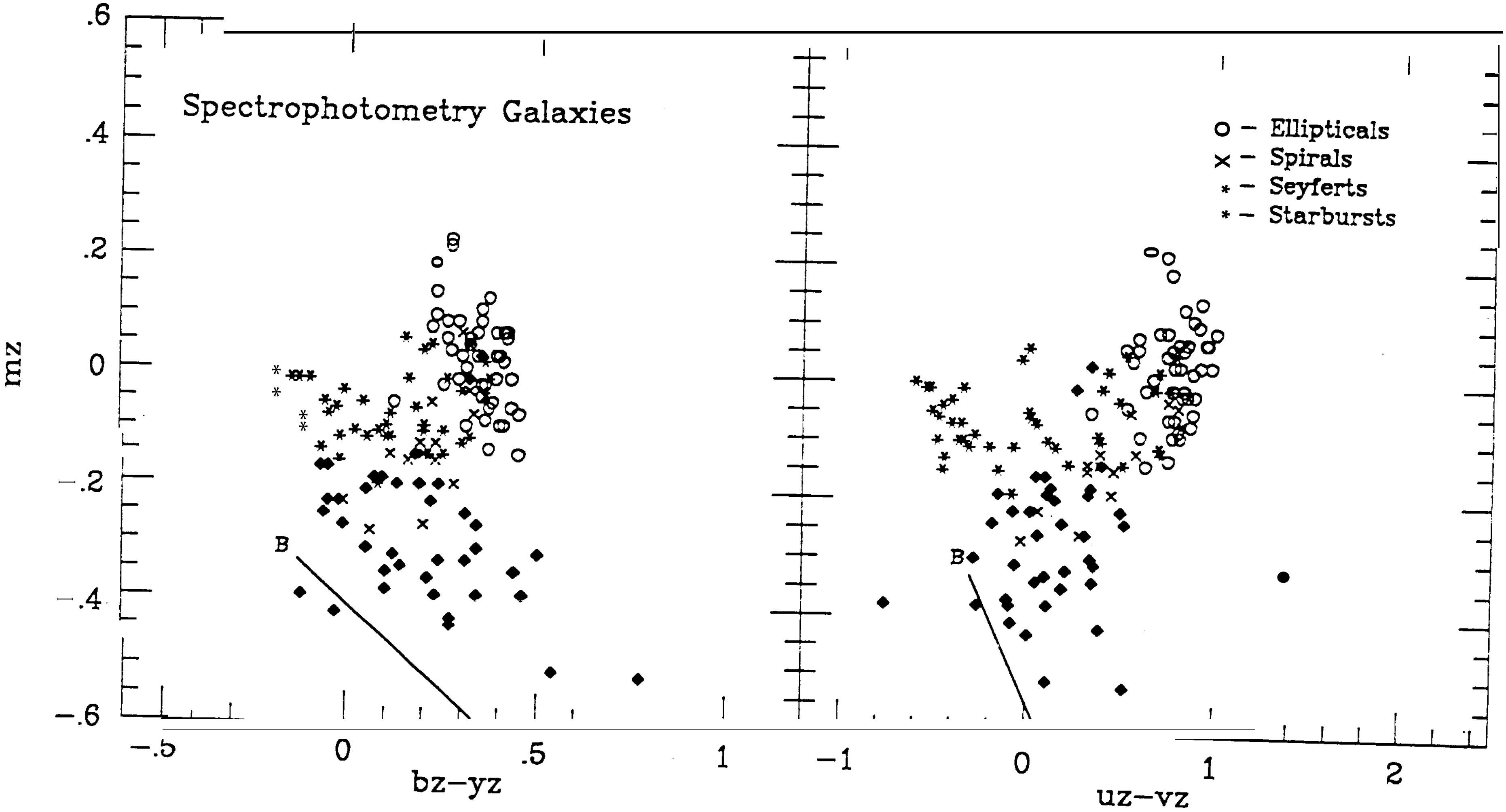
Spectrophotometry Galaxies
o – Ellipticals
x – Spirals
* – Seyferts
* – Starbursts
mz
.6
.4
.2
0
-.2
-.4
-.6
-.5
0
.5
1
-1
0
1
2
bz-yz
uz-vz
B
B

Figure 4

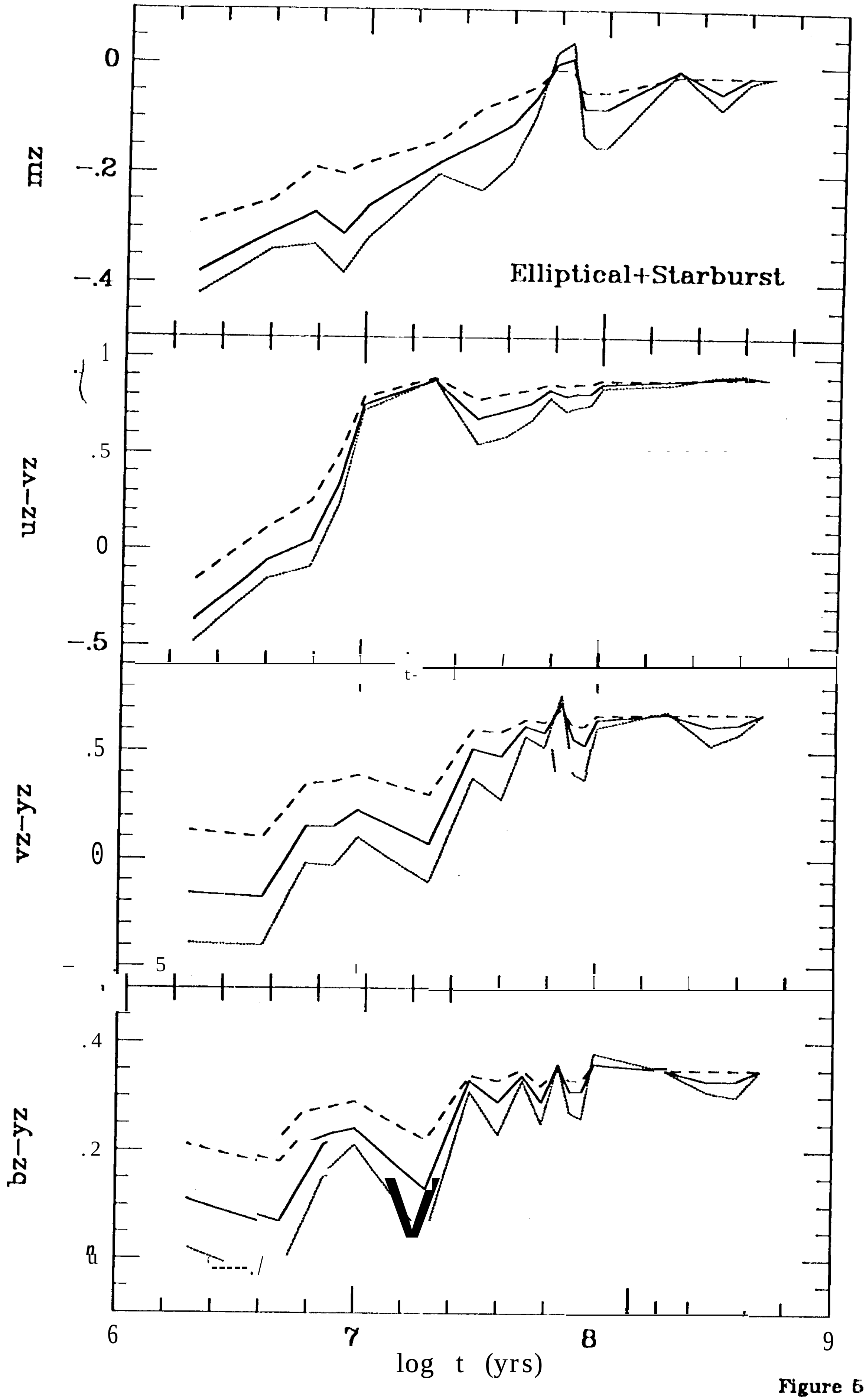

0
−.2
−.4
mz
Elliptical+Starburst
1
.5
0
−.5
uz−vz
.5
0
vz−yz
.4
.2
bz−yz
6
7
8
9
log t (yrs)

Figure 5

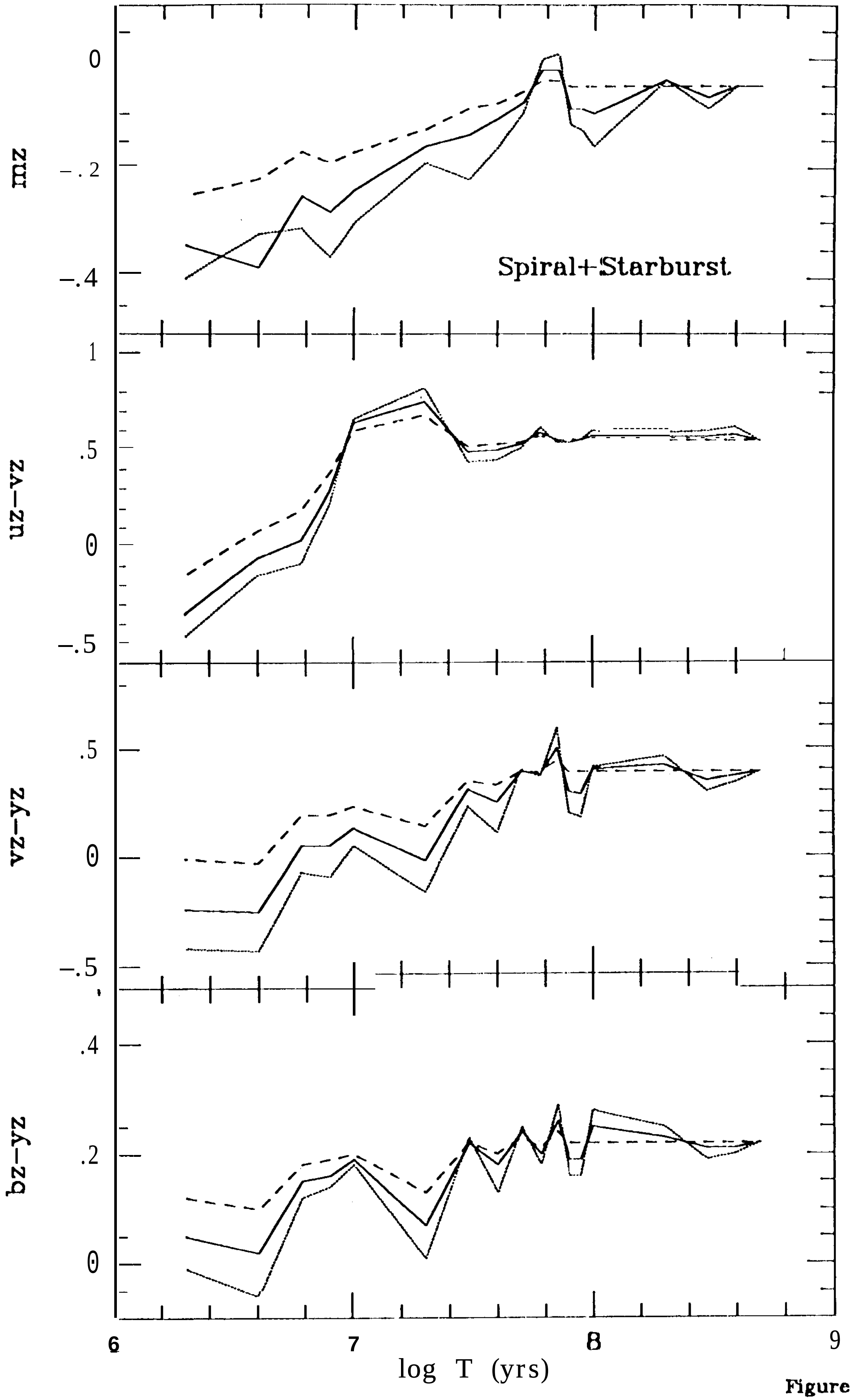

mz
0
-.2
-.4
Spiral+Starburst
uz-vz
1
.5
0
-.5
vz-yz
.5
0
-.5
bz-yz
.4
.2
0
6
7
8
9
log T (yrs)

Figure 6

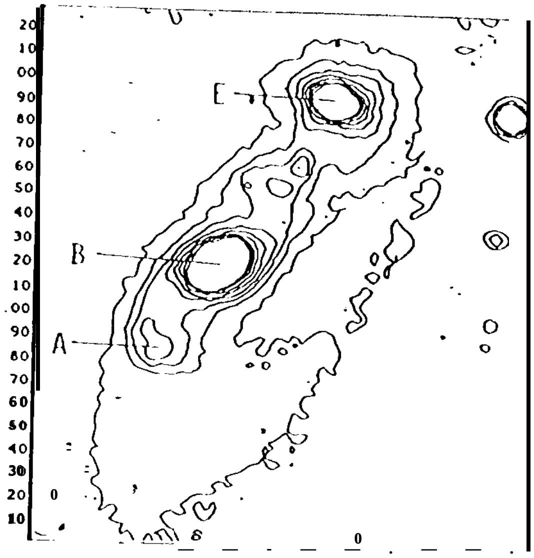

Arp 81

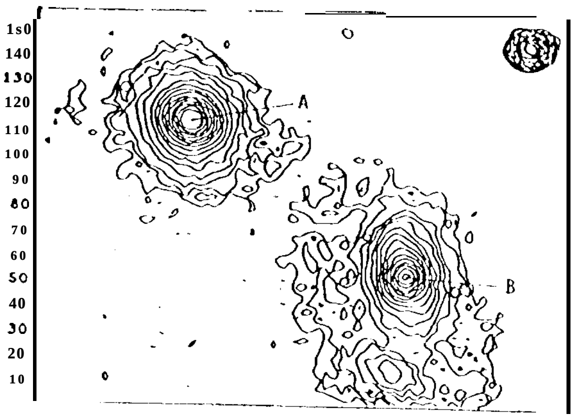

Arp 112

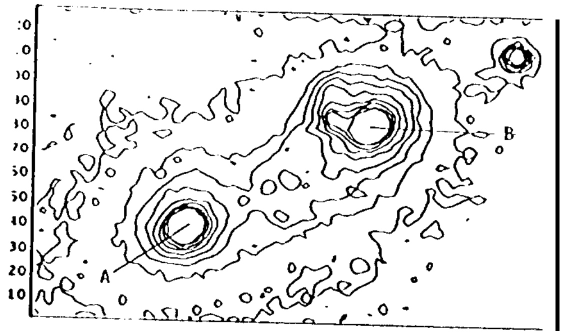

Arp 118

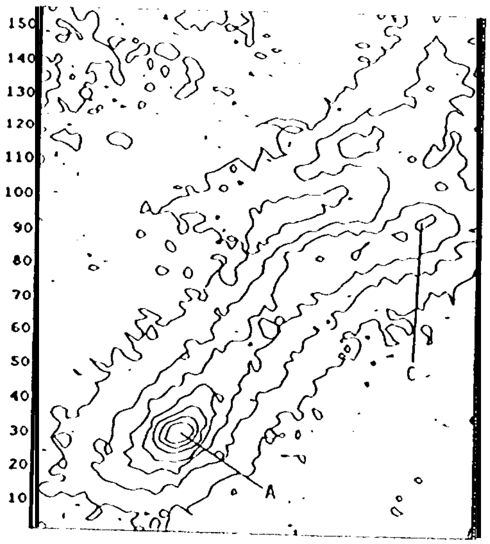

Arp 157

Figure '7a

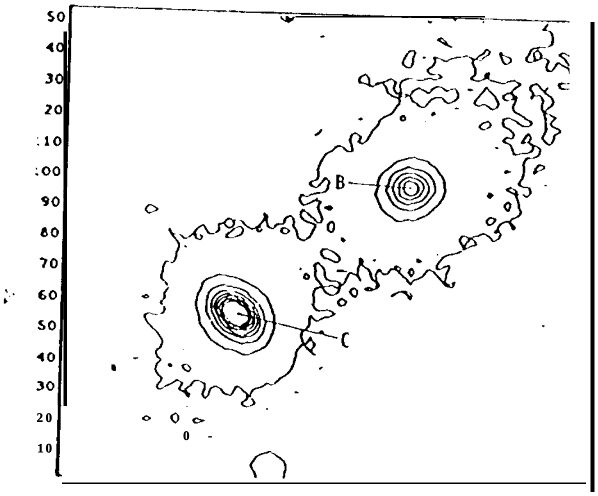

Arp 169

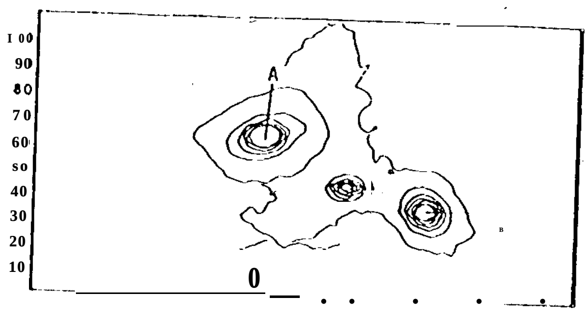

Arp 182

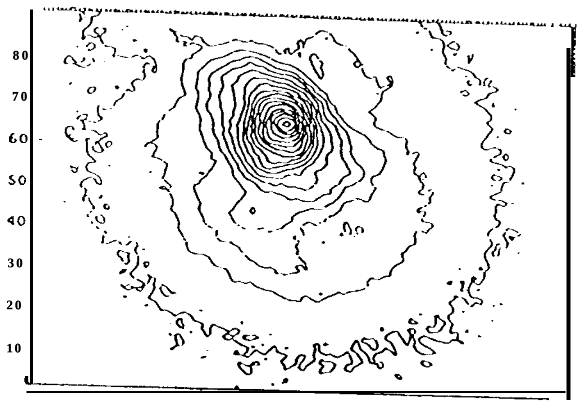

Arp 212

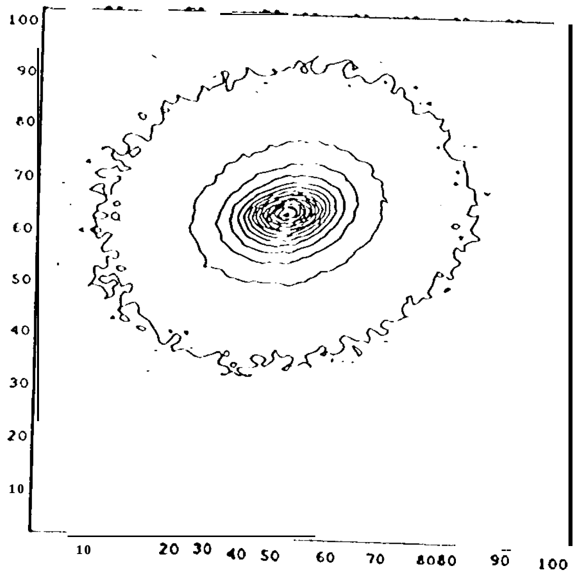

Arp 223

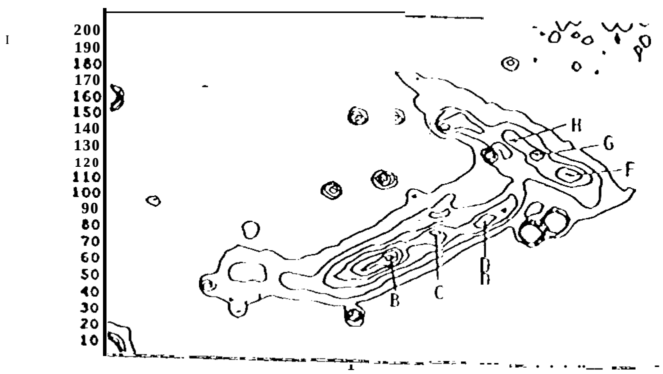

Arp 278

Figure 7b

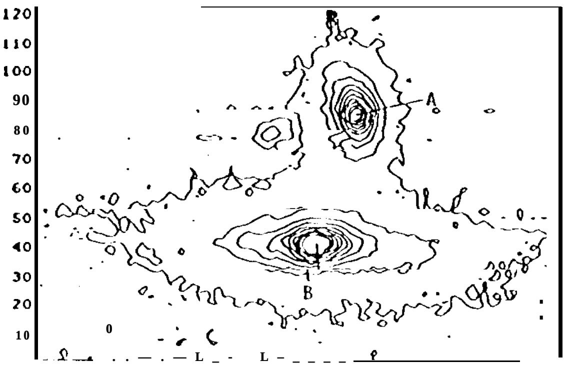

Arp 282

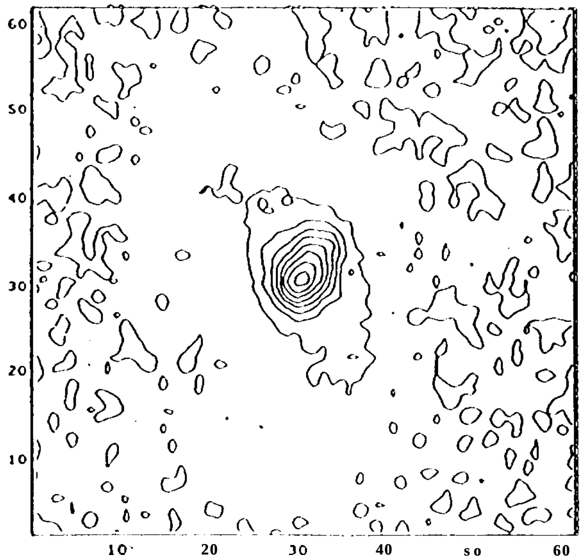

Mrk 309

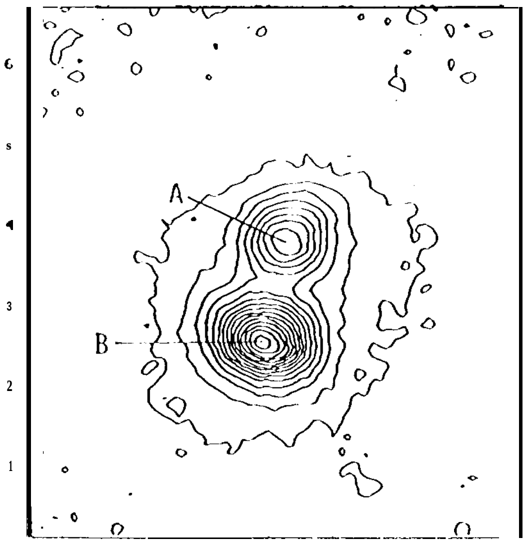

Mrk 480

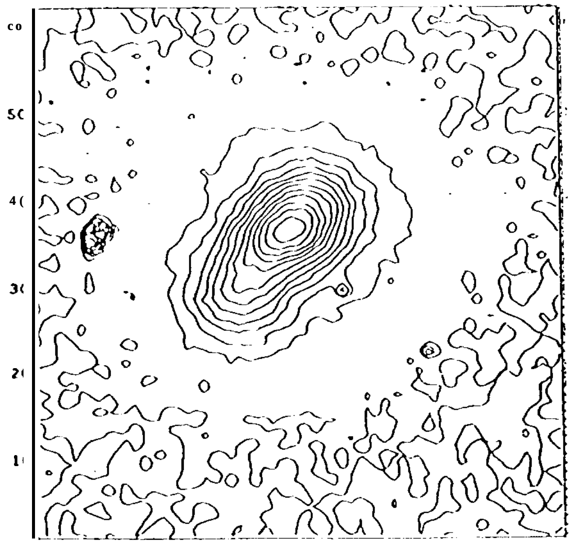

Mrk 496

Figure 7c

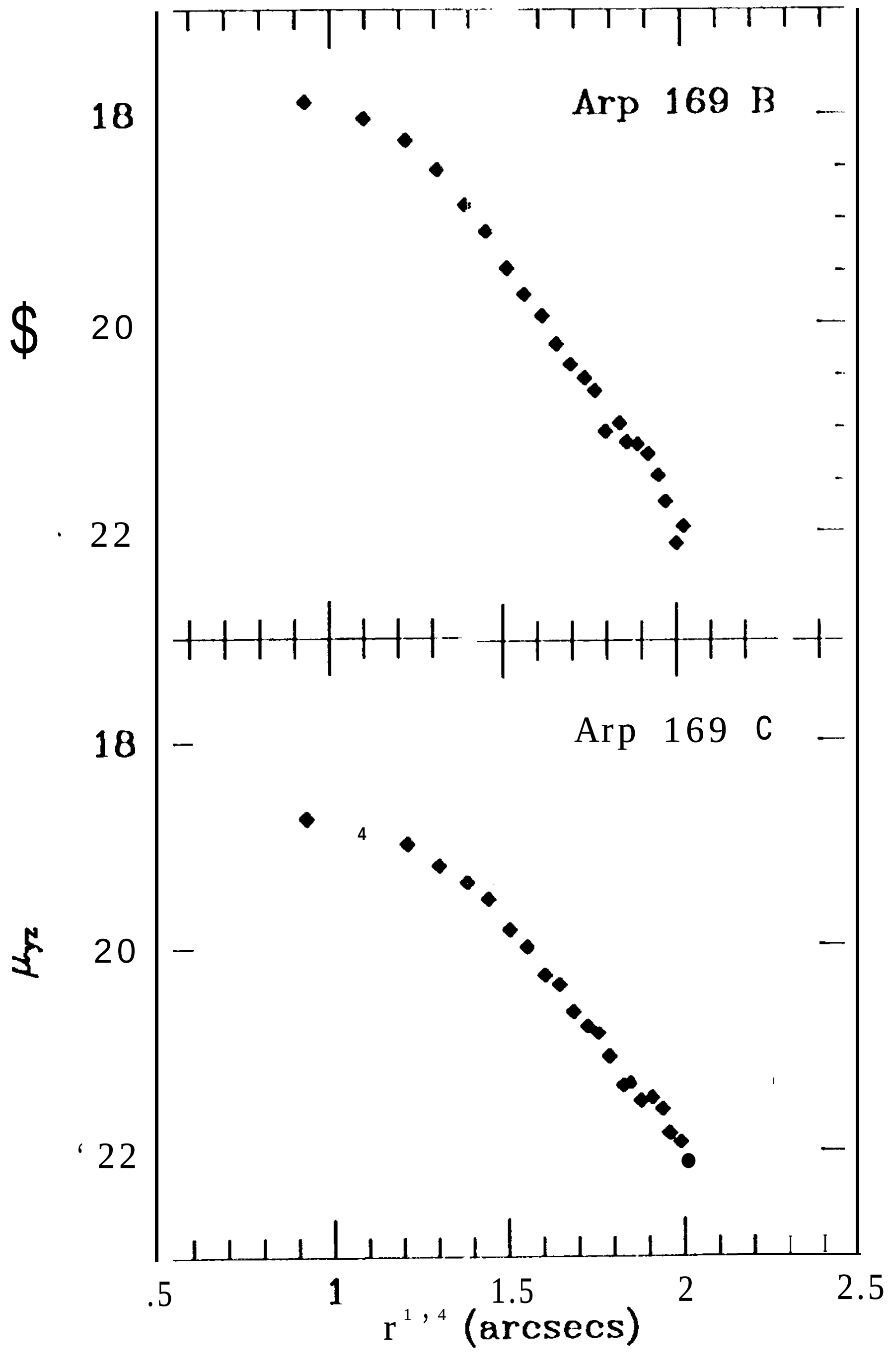

Figure B

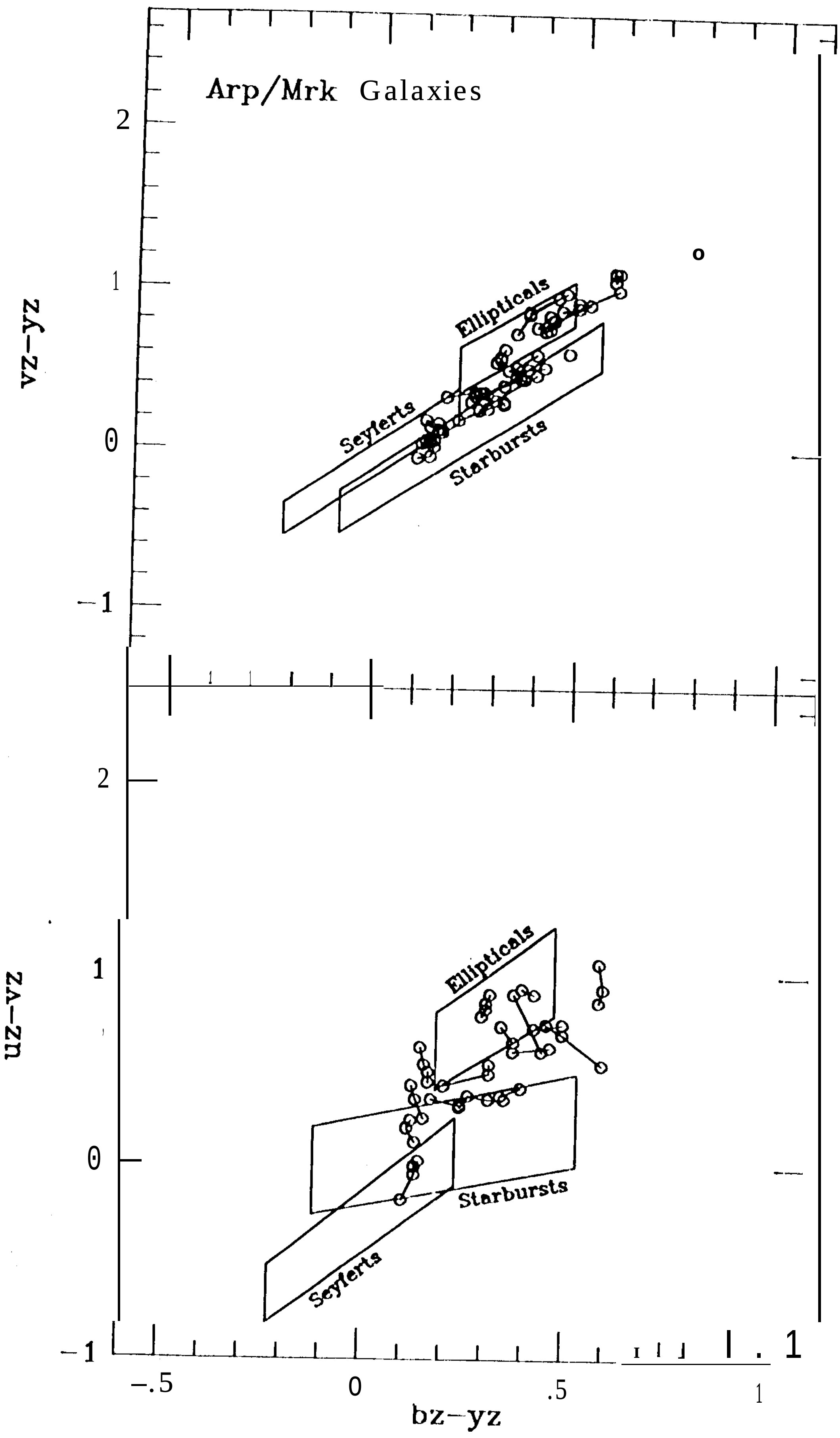

Arp/Mrk Galaxies
vz−yz
2
1
0
−1
Ellipticals
Seyferts
Starbursts
uz−vz
2
1
0
−1
Ellipticals
Starbursts
Seyferts
−.5
0
.5
1
bz−yz

Figure 9

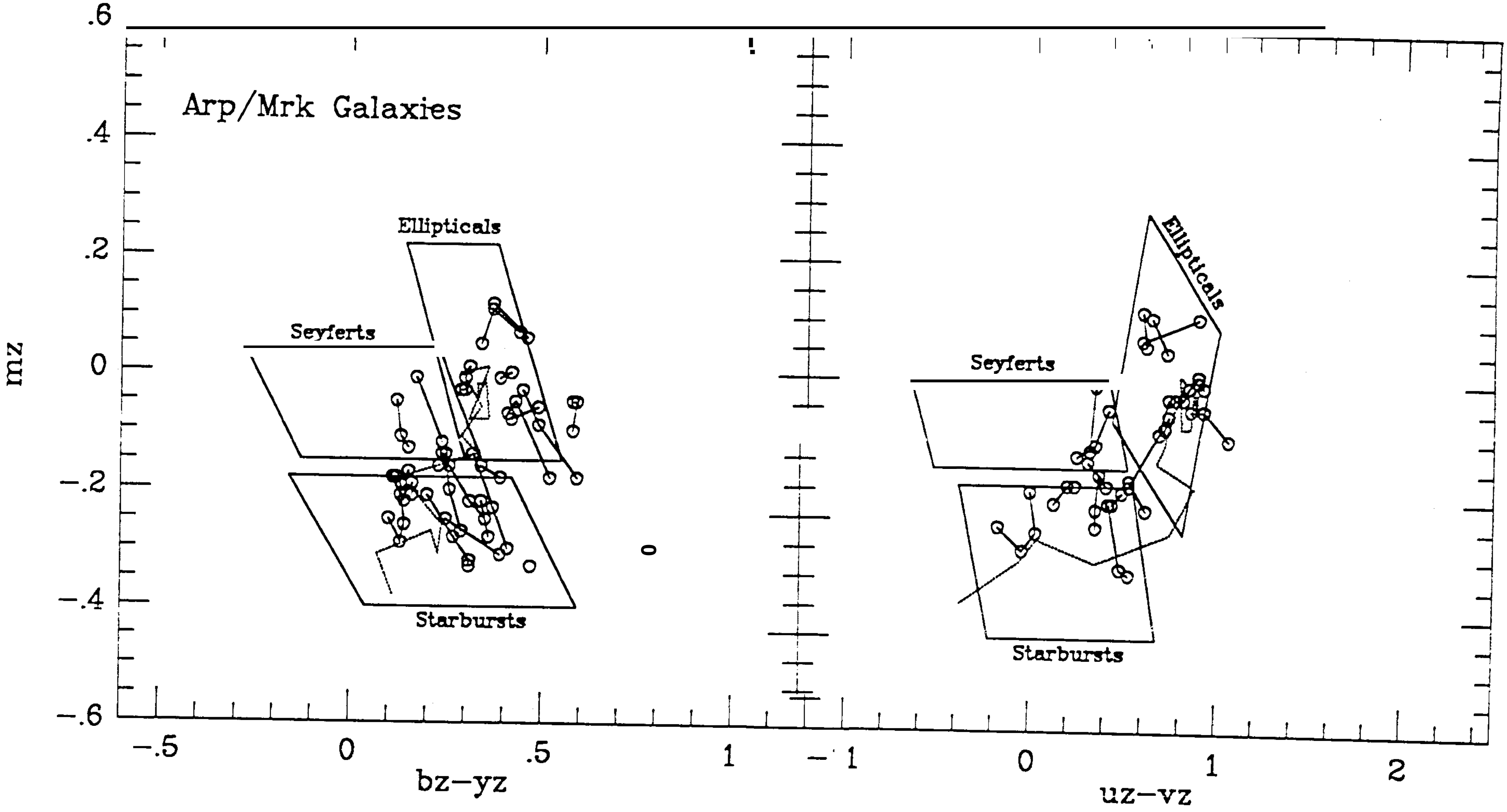
Arp/Mrk Galaxies
Ellipticals
Seyferts
Starbursts
Ellipticals
Seyferts
Starbursts
mz
bz−yz
uz−vz
.6
.4
.2
0
−.2
−.4
−.6
−.5
0
.5
1
−1
0
1
2

Figure 10

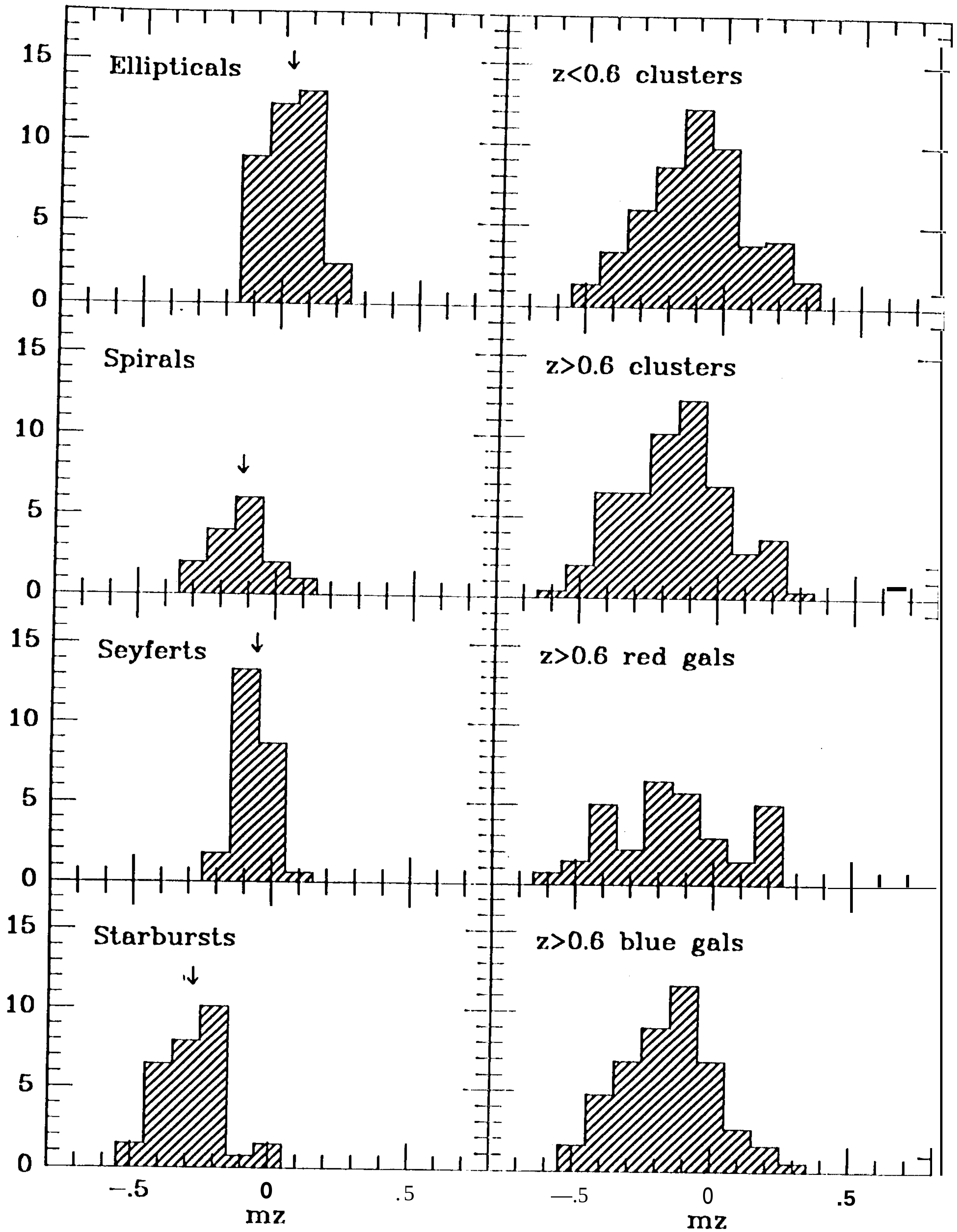

Ellipticals
z<0.6 clusters
Spirals
z>0.6 clusters
Seyferts
z>0.6 red gals
Starbursts
z>0.6 blue gals
15
10
5
0
−.5
0
.5
mz

Figure 11